Provided for non-commercial research and education use.
Not for reproduction, distribution or commercial use.

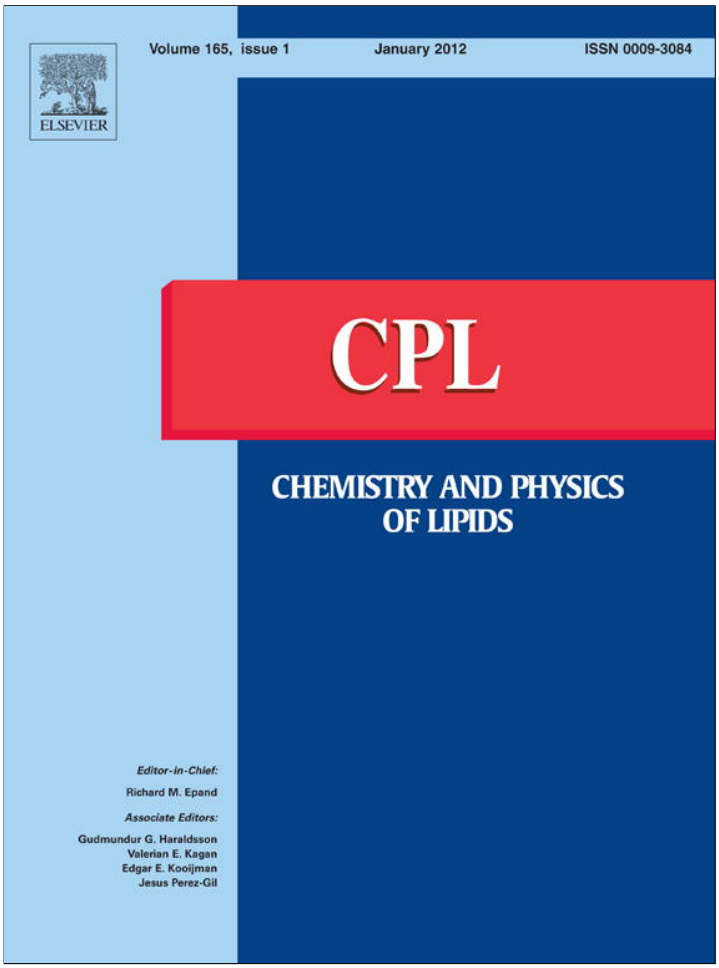

(This is a sample cover image for this issue. The actual cover is not yet available at this time.)

This article appeared in a journal published by Elsevier. The attached copy is furnished to the author for internal non-commercial research and education use, including for instruction at the authors institution and sharing with colleagues.

Other uses, including reproduction and distribution, or selling or licensing copies, or posting to personal, institutional or third party websites are prohibited.

In most cases authors are permitted to post their version of the article (e.g. in Word or Tex form) to their personal website or institutional repository. Authors requiring further information regarding Elsevier's archiving and manuscript policies are encouraged to visit:

http://www.elsevier.com/copyright

Author's personal copy

Chemistry and Physics of Lipids 165 (2012) 348–361

Contents lists available at SciVerse ScienceDirect

Chemistry and Physics of Lipids

journal homepage: www.elsevier.com/locate/chemphyslip

Dynamics and ordering of lipid spin-labels along the coexistence curve of two membrane phases: An ESR study

Andrew K Smith, Jack H. Freed*

Department of Chemistry and Chemical Biology, Baker Laboratory, Cornell University, Ithaca, NY 14853, United States

ARTICLE INFO

Article history:
Received 14 December 2011
Received in revised form 24 February 2012
Accepted 25 February 2012
Available online xxx

Keywords:
Liquid-ordered phase
Coexisting phases
Bilayer structure
Umbrella model
Condensing effect
Critical point

ABSTRACT

An analysis of electron spin resonance (ESR) spectra from compositions along the liquid-ordered (L_o) and liquid-disordered (L_d) coexistence curve from the brain-sphingomyelin/dioleoylphosphatidylcholine/cholesterol (SPM/DOPC/Chol) model lipid system was performed to characterize the dynamic structure on a molecular level of these coexisting phases. We obtained 200 continuous-wave ESR spectra from glycerophospholipid spin-labels labeled at the 5, 7, 10, 12, 14, and 16 carbon positions of the 2nd acyl chain, a sphingomyelin spin-label labeled at the 14 carbon position of the amide-linked acyl chain, a headgroup-labeled glycerophospholipid, a headgroup-labeled sphingomyelin, and the cholesterol analogue spin-label cholestane all within multi-lamellar vesicle suspensions at room temperature. The spectra were analyzed using the MOMD (microscopic-order macroscopic-disorder) model to provide the rotational diffusion rates and order parameters which characterize the local molecular dynamics in these phases. The analysis also incorporated the known critical point and invariant points of the neighboring three-phase triangle along the coexistence curve. The variation in the molecular dynamic structures of coexisting L_o and L_d compositions as one moves toward the critical point is discussed. Based on these results, a molecular model of the L_o phase is proposed incorporating the "condensing effect" of cholesterol on the phospholipid acyl chain dynamics and ordering and the "umbrella model" of the phospholipid headgroup dynamics and ordering.

© 2012 Elsevier Ireland Ltd. All rights reserved.

1. Introduction

According to the two-domain model of cholesterol-containing plasma membranes, the lipid bilayer consists of two coexisting liquid phases. The main biochemical effect of this biophysical model is the co-localization of reactive membrane proteins into lipid phase domains (Lingwood and Simons, 2010). Giant unilamellar vesicles composed of lipids from cell-derived plasma membranes have exhibited two coexisting liquid phases (Baumgart et al., 2007; Ayuyan and Cohen, 2008; Montes et al., 2007; Kaiser et al., 2009), but the partitioning of marker proteins between the two phase domains varied with the methods of vesicle preparation and were attributed to different lipid phase structure (by measuring "order") and protein compositions (Kaiser et al., 2009; Levental et al., 2011). Furthermore, it was proposed that lipid phase domains in biological membranes continuously vary in size, composition, and order mediated by proteins (Levental et al., 2011). These studies show that the two-domain model of biological membranes is likely true, but the detailed organization and structure of these lipid phases are dynamic, variable, and sensitive to both type and composition of membrane lipids and proteins.

While studies on lipid bilayers with the compositional complexity of biological membranes are desirable, a more precise description of lipid phase structure in terms of order and dynamics can be obtained on model lipid systems containing a few lipid species without the effects from proteins, although one would thereafter wish to include such effects. In simple binary and ternary model lipid systems containing cholesterol, studies have confirmed the existence of two distinct liquid phases, one being the cholesterol-rich liquid-ordered (L_o) phase and the other being the cholesterol-poor liquid-disordered (L_d) phase, and the coexistence regions of these two phases have been delineated for several ternary systems (Veatch and Keller, 2005; Goni et al., 2008; Feigenson, 2009; Marsh, 2009). At constant temperature and pressure the phase diagrams show that the lipid bilayer can consist of coexisting L_o and L_d phases with continuously varying composition (Smith et al., 2003; Veatch et al., 2004; Zhao et al., 2007), and that the molecular dynamics and ordering of these phases change with composition (Chiang et al., 2004; Swamy et al., 2006; Heberle et al., 2010). In describing lipid phase structure, order can either refer to the orientation of the lipid with respect to the bilayer normal or the degree of lipid packing, which varies from condensed to expansive; however, these two concepts are related in that a bilayer that is condensed and efficiently packed has lipids that are well oriented along the bilayer normal. In addition, the dynamics refers to the motion of the lipid with respect to its preferred alignment. A reasonable

* Corresponding author. Tel.: +1 607 255 3647; fax: +1 607 255 0595.
E-mail address: jhf3@cornell.edu (J.H. Freed).

0009-3084/$ – see front matter © 2012 Elsevier Ireland Ltd. All rights reserved.
doi:10.1016/j.chemphyslip.2012.02.009

Author's personal copy

assumption, which is generally true, is that dynamics and order are correlated, because the forces that condense the lipids hinder motion and inefficient packing causes free volume, which facilitates more rapid motion; however, in some cases, dynamics and ordering can be less correlated (Korstanje et al., 1989). The L_d phase is described as the state of the bilayer having fast phospholipid motions, rotational and translational, and acyl chains containing gauche bonds that reorient the chains away from the bilayer normal. On the other hand, the L_o phase is described as a state of the bilayer containing cholesterol that also has fast phospholipid motions, especially axial rotation around the bilayer normal, but acyl chains containing trans bonds that order the chains along the bilayer normal. The question still remains how the detailed dynamics and ordering of coexisting L_o and L_d phases for both the hydrophilic headgroup region and hydrophobic interior containing the phospholipid acyl chains change with varying composition, especially cholesterol, along the coexistence curve.

One of the well-known effects cholesterol has on phospholipid dynamics and ordering is called the condensing effect (Quinn and Wolf, 2009; Rog et al., 2009; Hung et al., 2007). The condensing effect of cholesterol is the non-ideal decrease in cross-sectional area per phospholipid with increasing cholesterol concentration (i.e. the decrease in area per phospholipid within the mixture is less than the sum of the areas per molecule from the pure states). A common definition of area per molecule from molecular simulations is the ratio of the total surface area of the mixture to the number of molecules, or to assume that the sterol ring of cholesterol is incompressible (i.e. its area is independent of its concentration), but the partial-specific-area formalism was found the best to demonstrate the condensing effect (Edholm and Nagle, 2005). The decrease in molecular area of the phospholipids is thought to be caused by the induction of trans bonds along the flexible acyl chains which orders them along the bilayer normal. Although the decrease in molecular area upon condensation is clear, the exact mechanism of the condensing effect is debatable with a few models being proposed, including condensed-complexes, template models, and the umbrella model (Radhakrishnan and McConnell, 1999; Daly et al., 2011; Huang et al., 1999). The condensed-complex and template models essentially rely on a stoichiometric chemical compound formation between phospholipid and cholesterol resulting from an ethalpic chemical reaction. During compound formation the acyl chains are extended in an all-trans configuration for a better physical bond with cholesterol, and the condensation results from the extended chains having a smaller cross-sectional area than without cholesterol.

The umbrella model was initially proposed to describe the maximum solubility of cholesterol in phosphatidylcholine bilayers (Huang et al., 1999). The umbrella model states that in a bilayer containing cholesterol the headgroups of the phospholipids move and orient in such a way as to shield the hydrophobic surface of cholesterol from water since the hydroxyl group of cholesterol is insufficient on its own; this expansion of the headgroup is concurrent with the condensation of the acyl chains to accommodate the insertion of cholesterol into both the hydrophobic part of the bilayer and at the interface. The umbrella model explains the condensing effect of cholesterol in that the headgroup motion is a cooperative action from the straightening of the acyl chains through trans bonds by cholesterol. Moreover, the degree of condensation or the strength of the interaction between phospholipid and cholesterol depends on both the degree of saturation of the acyl chains, the structure of the interface, which is postulated for the greater preference for sphingomyelin over phosphatidylcholines by cholesterol, and headgroup type (Mannock et al., 2010; Mainali et al., 2011a,b).

The goal of this study was to investigate the dynamics and ordering of the coexisting L_o and L_d phases from the SPM/DOPC/Chol model lipid system in detail. Samples were obtained at compositions along the known coexistence curve that also contain the locations of a critical point and invariant points to the neighboring three-phase region. A variety of phospholipid spin-labels labeled on the acyl chain or headgroup, along with a labeled cholesterol analogue, were used to see how the dynamics and ordering for all parts of the bilayer change with composition. The dynamic and order parameter profiles obtained from spectral analysis show the condensing effect of cholesterol and provide support for the umbrella model. We discuss this also in the context of the coexisting L_o and L_d compositions (i.e. those that are connected by tie-lines) as they approach the critical point.

2. Materials and methods

2.1. Materials

The phospholipids, brain-sphingomyelin (SPM) and dioleoylphosphatidylcholine (DOPC), and spin labels 1-palmitoyl-2-(5-doxyl stearoyl) phosphatidylcholine (5PC), 1-palmitoyl-2-(7-doxyl stearoyl) phosphatidylcholine (7PC), 1-palmitoyl-2-(10-doxyl stearoyl) phosphatidylcholine (10PC), 1-palmitoyl-2-(12-doxyl stearoyl) phosphatidylcholine (12PC), 1-palmitoyl-2-(14-doxyl stearoyl) phosphatidylcholine (14PC), 1-palmitoyl-2-(16-doxyl stearoyl) phosphatidylcholine (16PC), and dipalmitoylphophatidyl tempo (2,2,6,6,-tetramethyl-1-oxy) choline (DPPTC) were purchased from Avanti Polar Lipids, Inc. (Alabaster, AL). The chain-labeled SPM at the 14 carbon position, sphingosine-2-(14-doxyl palmitoyl) sphingomyelin (14SPM) and the headgroup-labeled SPM analogue (SPMHEAD), was synthesized at Nutrimed Biotech (Ithaca, NY). Cholesterol and the spin-labeled cholesterol analogue, 3β-doxyl-5α-cholestane (CSL) were obtained from Sigma-Aldrich (St. Louis, MO). Stock solutions of the lipids were prepared by diluting or dissolving the shipped stock in chloroform in a sealable vial. Purity > 99% of the lipid stock solutions was determined by thin-layer chromatography for phospholipids in chloroform/methanol/water = 65:25:4 (by volume) and hexane/diethyl ether/chloroform = 7:3:3 for cholesterol. All materials were used without further purification. The purity of stock solutions was checked every three months. The concentration of the phospholipid stock solutions was determined by a slightly modified procedure for the "determination of total phosphorous" published on Avanti Polar Lipid, Inc.'s website for technical information (http://www.avantilipids.com/TechnicalInformation.html). The concentration of the cholesterol stock solution was determined from an accurate mass (±0.1 mg) of the powdered cholesterol stock and the preparation of the solution in a 50 mL ± 0.05 volumetric flask.

2.2. Sample preparation and ESR spectroscopy

Spin-labeled lipid dispersions consisting of SPM, DOPC, and cholesterol were prepared as follows. Measured volumes of lipid stocks and the spin-label stock were dispensed using a Hamilton repeating dispenser into glass test tubes using a 50 μL Hamilton syringe to give the desired lipid compositions. The concentration of spin-label in the lipid dispersion was 0.2% of the total lipids (total amount of lipid = 2 μmol). These lipid-chloroform solutions were then converted to lipid-buffer suspensions by Rapid Solvent Exchange (Buboltz and Feigenson, 1999). The buffer used was 50 mMTris, 10 mMNaCl, and 0.1 mM EDTA at pH 7.0. The samples were stored under an argon atmosphere in the dark at room temperature for at least 24 h to reach equilibrium. After a few days the samples were centrifuged and the pellets were transferred to 1.5–1.8-mm-diameter × 100-mm-length glass capillaries with excess buffer. After the samples were centrifuged in the

Author's personal copy

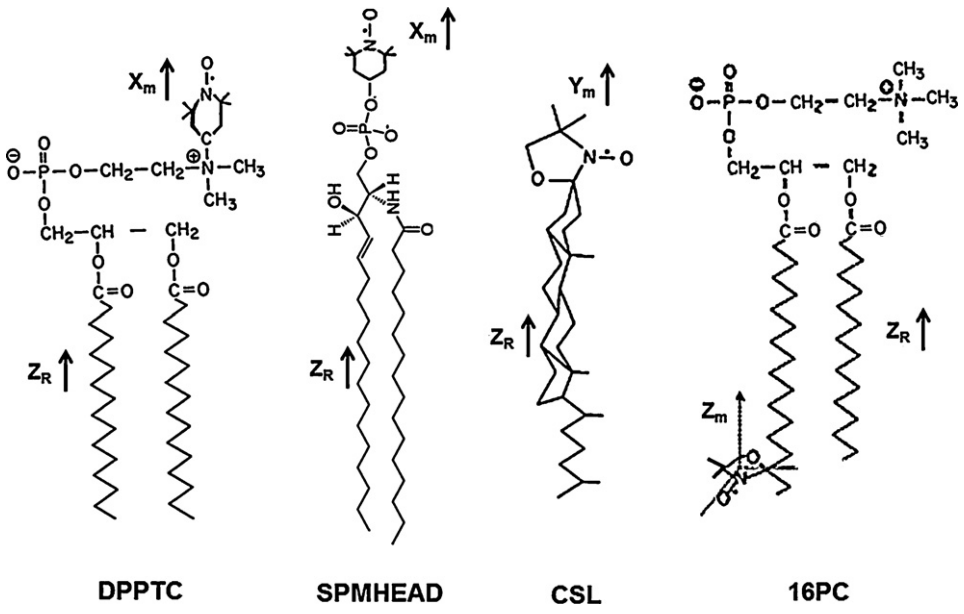

Fig. 1. The three main classes of lipid spin-labels. The *x*-ordered spin-labels ($X_m \,||\, Z_R$) are DPPTC and SPMHEAD, the *y*-ordered spin-label ($Y_m \,||\, Z_R$) is CSL, and the *z*-ordered spin-labels ($Z_m \,||\, Z_R$) are 5PC, 7PC, 10PC, 12PC, 14PC, 14SPM, and 16PC. Only the 16PC spin-label is shown but the other chain-labeled glycerophospholipids can be inferred. The spin-label 14SPM is not shown but it is palmitoyl-sphingomyelin with the nitroxide moiety attached at the 14 carbon of the amide-linked acyl chain.

capillaries, the supernatant (excess buffer) was removed to less than a millimeter above the pellet and the ends of the capillaries were flame sealed. Control experiments with select de-oxygenated samples using a glove box showed no significant change in spectra by oxidation of double bounds during sample preparation to measurement.

ESR spectra were obtained on a Bruker Instruments EMX ESR spectrometer at a frequency of 9.3 GHz at room temperature (~23 °C). The ESR capillary was placed inside a 2 mm NMR tube which was marked to position the sample pellet in the middle of the resonator. This configuration allowed for efficiency and consistency in switching samples, tuning, and sample measurements. The spectrometer settings for all samples were as follows: center field = 3477 G, sweep width = 120 G, microwave power = 2 mW, modulation frequency = 100 kHz, modulation amplitude = 0.5 G, resolution (points) = 1024. The number of scans for each spectrum varied, but the all spectra were adjusted with respect to magnetic field and normalized before analysis.

2.3. NLLS spectral fitting

The ESR spectra were analyzed in terms of the MOMD (microscopic-order macroscopic-disorder) model by a nonlinear least squares (NLLS) fitting method using theory based on the stochastic Liouville equation and the Levenberg-Marquadt search method of parameter space (Budil et al., 1996). The model contains four references frames interconvertible by rotational transformation: (1) the laboratory frame (X_L, Y_L, Z_L), with its *Z*-axis being defined as the static magnetic field direction; (2) the local director frame (X_d, Y_d, Z_d), which is the bilayer-orienting potential frame; (3) the molecular frame (X_R, Y_R, Z_R) in which the rotational diffusion tensor of the spin-label is diagonal; and (4) the magnetic tensor frame (X_m, Y_m, Z_m) in which the *g* and hyperfine (*A*) tensors are diagonal.

All spin-labels are labeled with a nitroxide moiety that carries the unpaired electron spin and for which the magnetic frame is defined accordingly with the X_m axis pointing along the N—O bond, the Z_m axis parallel to the 2pz axis of the nitrogen atom, and the Y_m axis perpendicular to the others. From the chemical structure and previous studies, all spin-labels used fall into three different classes based on the orientation of the magnetic frame with the molecular frame (Fig. 1): the acyl chain labeled phospholipids (5PC, 7PC, 10PC, 12PC, 14PC, 14SPM, 16PC) are called *z*-ordered (i.e. the Z_m axis is parallel to the Z_R axis, $Z_m \,||\, Z_R$) (Swamy et al., 2006; Ge et al., 1999, 2003; Ge and Freed, 2011), CSL is *y*-ordered (i.e. $Y_m \,||\, Z_R$) (Ge et al., 1999, 2003; Barnes and Freed, 1998), and the headgroup-labeled phospholipids DPPTC (Ge and Freed, 2011, 1998, 2009) and SPMHEAD (Ge et al., 1999), which is very similar to dipalmitoylphospho-tempo (DPP-Tempo) (Ge and Freed, 2009, 2003) are *x*-ordered ($X_m \,||\, Z_R$). Because of the quasi two-dimensionality of lipid bilayers and each local layer consisting of oriented lipids, the molecular frame is related to the local director frame via a potential energy function describing the orientation of the spin-label with respect to the bilayer normal (i.e. the Z_d axis). The MOMD model describes the structure of lipid molecules (including the spin-labels) within a vesicle dispersion in that the molecules have a preferred local orientation (i.e. along the bilayer normal), but the vesicles in which the molecules reside are closed bilayers, so globally the molecules have random orientations. Operationally, the fitting procedure using the MOMD model involves first calculating a spectrum for each orientation of the bilayer normal with respect to the static magnetic field (i.e. the angle between Z_d and Z_L is Ψ) chosen randomly a pre-defined number of times from a uniform distribution of orientations from 0 to π (25 randomly chosen orientations were chosen in this study) and then the final spectrum for the sample is the average of these spectra.

The two parameter sets used to fit the ESR spectra were the fixed principal components of the magnetic tensors and the variable dynamic and order parameters. The *g* and *A* tensor parameters were taken from the literature (Ge et al., 1999, 2003; Ge and Freed, 1998; Earle et al., 1994; Kurad et al., 2003) and shown in Table 1. The magnetic parameters were fixed for each spin-label when fitting the samples around the coexistence curve independent of the composition of the sample because these parameters were observed to change little with cholesterol concentration (Kurad et al., 2003). For the chain-labeled spin-labels a simple linear dependence with carbon position along the acyl chain was assumed for the *A* tensor components (Table 1); however, the *g* tensor components used

Author's personal copy

Table 1
The magnetic *g* and *A* tensors for the three classes of lipid spin-labels used in this study.

Class	g_{xx}[a]	g_{yy}[a]	g_{zz}[a]
Chain-labeled (*z*-ordered)	2.0086	2.0058	2.0020
CSL (*y*-ordered)	2.0020	2.0086	2.0058
Headgroup-labeled (*x*-ordered)	2.0058	2.0020	2.0086

Class	Carbon position	A_{xx}	A_{yy}	A_{zz}
Chain-labeled[b]	5	5.5	5.5	33.6
	7	5.4	5.4	33.4
	10	5.3	5.3	33.2
	12	5.2	5.2	33.0
	14 (PC & SPM)	5.1	5.1	32.8
	16	5.0	5.0	32.6
CSL[c]		34	5.8	5.8
Headgroup-labeled[d]		5.6	34.5	5.6

The magnetic *g* and *A* tensors for the three classes of lipid spin-labels used in this study were obtained from the literature.

[a] For X-band ESR spectra the *g* tensor is not as crucial to the fitting as the *A* tensor, so values were chosen within observed bounds for the *z*-ordered spin-labels (Ge et al., 2003; Earle et al., 1994; Kurad et al., 2003) and cyclically permuted for the *x*-ordered and *y*-ordered spin-labels.

[b] Values were from Ge et al. (1999, 2003), and a linear change with increasing carbon position was assumed for simplicity.

[c] Values were from Ge et al. (2003).

[d] Values were from Ge and Freed (1998) and Ge et al. (1999).

were the same for all chain-labeled spin-labels. The classes of spin-labels (i.e. *z*-ordered, *y*-ordered, and *x*-ordered) are related to each other by a cyclical permutation, which was performed before fitting the spectra so that the Z_R becomes the principal axis for rotation and ordering. The variable parameter set consists of the principal components of an axially symmetric rotational diffusion tensor for the spin-label molecule (called $R_\perp$ and $R_{||}$), the coefficients for the potential of mean torque (called $c20$ and $c22$), and the gaussian inhomogeneous broadening parameters (called gib0 and gib2). The expression for total broadening has the following form (Budil et al., 1996):

$$\text{gib} = \text{gib0} + \text{gib2} \times \cos^2(\Psi) \quad (1)$$

The second term applies to the MOMD model and refers to the variation in inhomogeneous broadening caused by different orientations of the spin-label director relative to the static magnetic field. The important dynamic parameters, $R_\perp$ and $R_{||}$, describe the motion of the spin-label assuming axial symmetry, with $R_{||}$ being the rotational rate around Z_R (i.e. the long axis of the molecule), and $R_\perp$ being the rotational rate around an axis perpendicular to Z_R. The potential energy parameters, $c20$ and $c22$, are used to calculate the two order parameters of the spin-label, S_0 and S_2 (Chiang et al., 2004). S_0 measures the extent of alignment of Z_R with respect to the bilayer normal Z_d and S_2 measures the extent to which there is a preferential alignment of the other molecular axes (X_R versus Y_R) with respect to Z_d.

2.4. Sample compositions and fitting procedure

ESR spectra for all 10 spin-labels were obtained at 20 sample compositions that lie on the coexistence curve for the $L_o + L_d$ coexistence region of the SPM/DOPC/Chol phase diagram (Fig. 2). The coexistence curve was known from previous studies with an estimated uncertainty between 2% and 5% (Smith et al., 2003; Smith and Freed, 2009). Compositions on the coexistence curve exist at the edge of one phase, either L_o or L_d, and compositions within the coexistence region exist as two coexisting phases, with the compositions of the coexisting phases given by the tie-line field (i.e. the infinite set of all tie-lines). The tie-line field for the $L_o + L_d$ coexistence region of the SPM/DOPC/Chol phase diagram was recently determined and is shown in Fig. 2 (Smith and Freed, 2009). The data used for the tie-line field determination was 50 16PC spectra within the coexistence region and 20 16PC spectra along the coexistence curve (the same analyzed in this work). The outer hyperfine splittings of the 16PC spectra along the coexistence curve were used to delineate two key phase transition regions, which are the critical

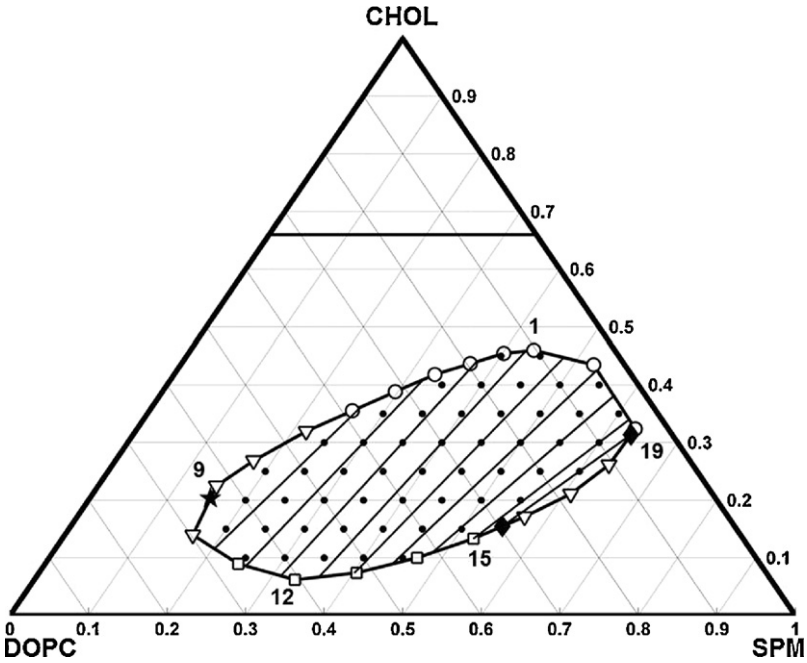

Fig. 2. The tie-line field and $L_o + L_d$ coexistence curve of the SPM/DOPC/Chol phase diagram. 50 16PC spectra (black dots) and 20 16PC spectra (circles, triangles, and squares) were used in a previous study (Smith and Freed, 2009) to determine the tie-line field (black lines), a process that yielded the critical point (star) and the three-phase invariant points (diamonds). Using the critical point and invariant points, the coexistence curve is divided into the L_o phase boundary (compositions 19, 20, 1–9), the L_d phase boundary (compositions 10–15), and the three-phase region (compositions 16, 17, 18).

Author's personal copy

point region (CPR) and the end tie-line region (ETR). In determining the tie-line field the critical point and the three-phase invariant points (i.e. end points of the end tie-line bordering the three-phase region) were then located.

Since the compositions on the coexistence curve exist as a single phase, the ESR spectra were analyzed as having only one spectral component. By varying the dynamic parameters ($R_\perp$ and $R_{||}$), the potential energy parameters ($c20$ and $c22$), and the broadening parameters (gib0 and gib2) a careful assessment of the best fit to the spectrum at sample 1 was obtained first. Then the parameters of this fit were used as a "seed" or initial parameter set for both sample 2 and sample 20. The procedure of using the parameter set obtained from fitting the previous spectrum to seed the following spectrum was repeated around the coexistence curve until all spectra have been fit. This fitting procedure provided a consistent set of results, despite the ambiguity caused by the limited resolution of MOMD spectra. We require that the parameters obtained from the fit vary smoothly and consistently with composition. This strategy has been successfully employed in fitting spectra varying with temperature (Ge and Freed, 2003). We did not, in this work, perform a multi-frequency ESR study, which has the potential to resolve some of the ambiguities we encountered in this single frequency study (Barnes and Freed, 1998; Lou et al., 2001; Zhang et al., 2010).

3. Results and discussion

The experimental and theoretical (fitted) spectra are provided in Supplementary Material. We refer to a parameter profile as a dynamic or order parameter, obtained from the fits, plotted against sample number, which refers to the sample composition as shown in Fig. 2. Using the known critical point and adjacent three-phase region (Fig. 2), the parameter profiles are divided up into L_o phases (sample numbers 1–9 and 19–1) and L_d phases (sample numbers 9–15). Because sample numbers 16, 17, and 18 lie within the three-phase coexistence region, the fit parameters from this region were excluded from interpreting the dynamics and ordering of the coexisting L_o and L_d phases.

The dynamic fitting parameters (i.e. $R_\perp$ and $R_{||}$) and the order parameters (i.e. S_0 and S_2) obtained from the potential energy fitting parameters have a simple physical interpretation. The greater the value of $R_\perp$ and $R_{||}$, the faster the rotation, and therefore the less "friction" the nitroxide moiety experiences to its movement. This reflects packing constraints (i.e. availability or lack of free volume) or pressure fields (i.e. the condensing effect can be seen as a lateral pressure compacting cholesterol and phospholipid closer together). The order parameters refer to the alignment of the nitroxide, through the main lipid molecular axis (Z_R), with the bilayer normal; therefore, generally, the higher the ordering the more restricted is the range of motion relative to the bilayer normal. The degree to which the behavior of the nitroxide reflects the behavior of the lipid to which it is attached depends on the substantial rigidity of the attachment; therefore, although the dynamic and order parameters report directly on the state of the nitroxide moiety, the physical structure of the bilayer can still be inferred.

For the chain-labeled spin-labels, the nitroxide moiety is rigidly attached to one of the carbons of the 2nd acyl chain (Fig. 1). Therefore, the motion and orientation of the nitroxide predominantly depends on the local gauche/trans bond distribution along the acyl chain. Generally, trans bonds orient the acyl chain more with the bilayer normal tending to yield a large S_0 and gauche bonds (along with cis double bonds) orient the acyl chains more with the perpendicular to the bilayer normal, lowering S_0. Note that, in this latter case, a negative S_0 is obtained in the limit of perpendicular alignment of Z_R with the bilayer normal (Chiang et al., 2004), although in our case chain dynamics tend to reduce the value of a positive S_0. The S_2 order parameter distinguishes a difference in ordering of X_R and Y_R with respect to the membrane normal but also tends to absorb effects of the limits of the MOMD model. It should be noted that with X-band ESR spectra the order parameters reflect a composite of fast and slow motions (Lou et al., 2001); the fast methylene bond rotations and the slower rotation of the entire acyl chain and the phospholipid.

For the headgroup-labeled spin-labels the nitroxide moiety is not rigidly attached to the headgroup (Fig. 1); therefore, the relevant interpretation of the dynamics and order parameters in terms of the motion and orientation of the entire headgroup is less clear. However, because of the large damping effect of the aqueous medium, a high correlation between the motions of the nitroxide and the whole headgroup is assumed (Ge and Freed, 2003). Lastly, unlike the chain-labeled and headgroup-labeled spin-labels, the dynamic and order parameters for CSL more directly reflect the molecule as a whole, since the nitroxide moiety of CSL is rigidly attached to the sterol ring system (Fig. 1).

With these physical interpretations of the dynamic and order parameters, we can interpret our results for the compositions around the $L_o + L_d$ coexistence curve.

3.1. Dynamic structure of L_o and L_d phases

3.1.1. The chain-labeled spin-labels

3.1.1.1. $R_\perp$ profiles. The $R_\perp$ profiles for all chain-labeled spin-labels (i.e. 5PC, 7PC, 10PC, 12PC, 14PC, 14SPM, and 16PC) are plotted in Fig. 3. For all compositions $R_\perp$ increases with increasing carbon position on the acyl chain. However, the range of $R_\perp$ is greater for the L_o phase than the L_d phase. For example, for the L_o phase with the highest cholesterol concentration (composition1, mole fraction cholesterol ~45%), the change in $R_\perp$ between 5PC and 16PC is ca. a factor of 10, whereas for the L_d phase with the lowest cholesterol concentration (composition 12, mole fraction cholesterol ~5%), the change is ca. a factor of 5. This indicates that the free volume near the end of the acyl chains is greater than near the interface for both the L_o and L_d phase; however, the difference between these two locations is greater for the L_o phase than the L_d phase. This results because the change in $R_\perp$ with composition for the top half of the acyl chain does not depend on the type of phase, whereas the change with composition for the bottom half of the acyl chain does depend on the type of phase.

In the L_o phase with decreasing cholesterol and increasing DOPC (compositions 1–9), $R_\perp$ increases greatly for 5PC and 7PC, increases slightly for 10PC and 12PC, and remains relatively constant with a slight decrease for 14PC. But it decreases and then levels off for 14SPM and 16PC as the L_o compositions approach the critical point. In the L_o phase with increasing cholesterol and decreasing SPM (compositions 19–1), $R_\perp$ decreases or remains constant for 5PC, 7PC, and 10PC, but increases for 12PC, 14PC, 14SPM, and 16PC. This seemingly counter-intuitive result of a decrease (increase) in $R_\perp$ at the end of the acyl chain with decreasing (increasing) cholesterol content was also observed for 16PC within the L_o phase in the DPPC/DLPC/Chol model system (Chiang et al., 2004) and between DMPC and a 1/1 DMPC/cholesterol mixture (Mainali et al., 2011a,b). In the DOPC-rich L_d phase with decreasing cholesterol but increasing SPM (compositions 9–12), $R_\perp$ increases for all spin-labels except for 12PC, which remains approximately constant. In the L_d phase with increasing cholesterol and SPM (compositions 12–15), $R_\perp$ decreases for all spin-labels except for 14PC, which remains approximately constant.

In summary, for the top half of the acyl chain, $R_\perp$ increases with decreasing cholesterol (compositions 1–12) and decreases with increasing cholesterol (compositions 12–20). This result for the top half of the acyl chains for both the L_o and L_d phases is consistent with the condensing effect, in which the free volume increases with

Author's personal copy

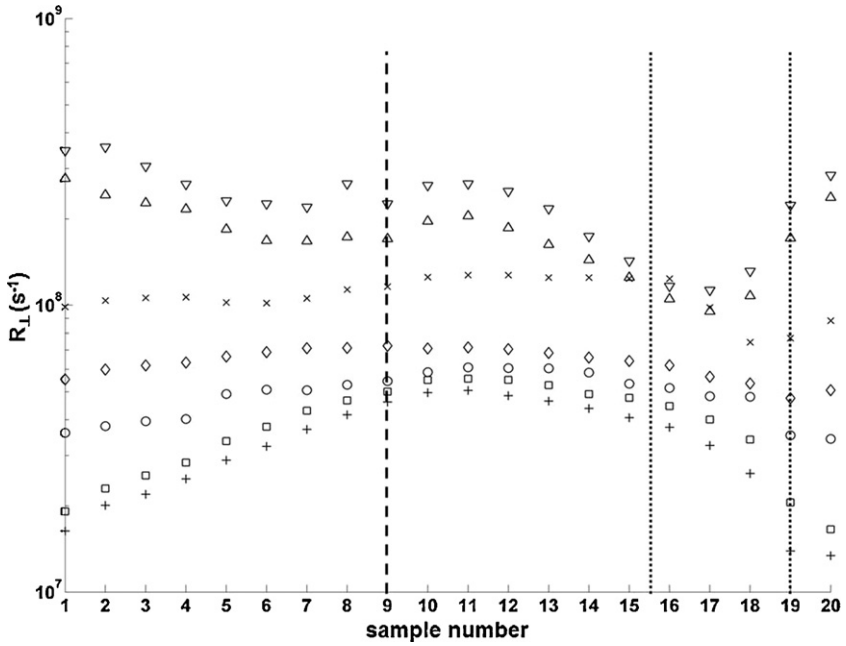

Fig. 3. The $R_\perp$ parameter (log-scale) profiles for the chain-labeled phospholipids. 5PC (plus sign), 7PC (squares), 10PC (circles), 12PC (diamonds), 14PC (crosses), 14SPM (up triangles), and 16PC (down triangles). The dashed line is the location of the critical point and the dotted lines are the locations of the invariant points of the three-phase region.

decreasing cholesterol and vice versa. However, for the bottom half of the acyl chains, especially at the ends, $R_\perp$ generally increases (decreases) with increasing (decreasing) cholesterol in the L_o phase and increases (decreases) with decreasing (increasing) cholesterol in the L_d phase. Therefore, within the L_o phase, while the top condenses, the bottom expands, and within the L_d phase, the top and bottom condense (expand) together. Furthermore, the shape of the profiles for 14SPM and 16PC are basically the same, although $R_\perp$ was slower for 14SPM, but shape of the profiles for 14SPM and 14PC are different. Differences between 14SPM and 14PC were also observed and attributed to partial interdigitation and the asymmetry of the acyl chains lengths because of their different attachment at the interface, in which the sn-2 chain of 14PC is a shorter than the sn-1 chain and the N-acyl chain of 14SPM is longer than the sphingosine chain (Veiga et al., 2001; Collado et al., 2005).

3.1.1.2. $R_{||}$ profiles. The $R_{||}$ parameter is typically very fast for phospholipid acyl chains, and when the rotational rate is much greater than the anisotropic *g* & *A*-tensors, the fitting is not very sensitive to that parameter. This was the case for 10PC, 12PC, 14PC, 14SPM, and 16PC; therefore, a more detailed analysis of these profiles with composition was unjustified (they can be found in Supplementary Material). However, the $R_{||}$ profiles for 5PC and 7PC were sensitive to the fits and, for comparison, were plotted with the $R_\perp$ profiles for these spin-labels in Fig. 4. For all compositions $R_{||} < R_\perp$ for 5PC and 7PC, in contrast to all cases lower down the chain. In addition, a pronounced opposite trend with composition exists between the two parameters for both 5PC and 7PC. (We checked that this was not due to any significant correlation between these parameters in the fitting procedure.) Also, the two rotational parameters near the top of the acyl chain are clearly a function of cholesterol concentration regardless of phase. $R_\perp$ increases with decreasing cholesterol (compositions 1–12) and decreases with increasing cholesterol (compositions 12–20), and $R_{||}$ decreases with decreasing cholesterol and increases with increasing cholesterol.

As mentioned previously, the cholesterol dependence of $R_\perp$ likely results from the condensing effect on the phospholipids. However, the expectation is that the condensation would slow the axial rotation of the acyl chains (i.e. $R_{||}$) with increasing cholesterol and speed up with decreasing cholesterol, but the opposite is observed. A possible explanation is that cholesterol acts as a "spacer" pushing the phospholipids apart and decreasing their interactions both with the acyl chains and headgroups; therefore, the phospholipids and/or acyl chains are freer to rotate. Another explanation is that cholesterol acts like a lubricant that decreases the "friction" of axial rotation, and would imply an absence of compound formation between SPM and cholesterol.

The fact that we find $R_{||} < R_\perp$ for 5PC and 7PC might, at first, seem surprising, but this has previously been observed in a MD simulation combined with experiment, on ^{31}P relaxation, from which $R_{||}/R_\perp \cong 0.1$ for the upper portion of the acyl chains (Klauda et al., 2008). This was explained by $R_{||}$ being retarded by the strong interactions (e.g. hydrogen-bonds and salt bridges) at the lipid/water interface. In a previous study, from this laboratory (Swamy et al., 2006) it was assumed that $R_{||}$ was very fast, so that the spectra were insensitive to it. Thus no attempt was made to vary $R_{||}$ for 5PC and 7PC, as we have done in the present study, and which has unequivocally yielded $R_{||} > R_\perp$ at these positions. In another study (Livshits et al., 2004), on a different lipid system, where they obtained 9 GHz and 94 GHz spectra, their analysis yielded a result whereby $R_{||}$ approaches $R_\perp$ in value as one proceeds up the chain, which is in this sense consistent with our results. However, that work used a special wobbling-in-a-cone model and an assumption of motional narrowing to obtain partially averaged *g* and *A* tensors from the 94 GHz spectra before fitting the 9 GHz spectra using MOMD. It would be more appropriate, however, to simultaneously fit spectra at both frequencies, especially since at 94 GHz the slower overall motions still contribute to the spectrum, and at the higher frequencies slow motional analysis is more appropriate (Lou et al., 2001; Zhang et al., 2010). In fact, a more advanced model (SRLS) was employed by Lou et al. (2001) to separate local from overall motions from combined 250 GHz and 9 GHz spectra. They found even for 16PC, for the local motions, that $R_{||}^L < R_\perp^L$. In the present work wherein we extensively used just 9 GHz spectra, it was necessary to confine our fitting to the simpler MOMD model, as we have described above. In this case one obtains a composite of local

Author's personal copy

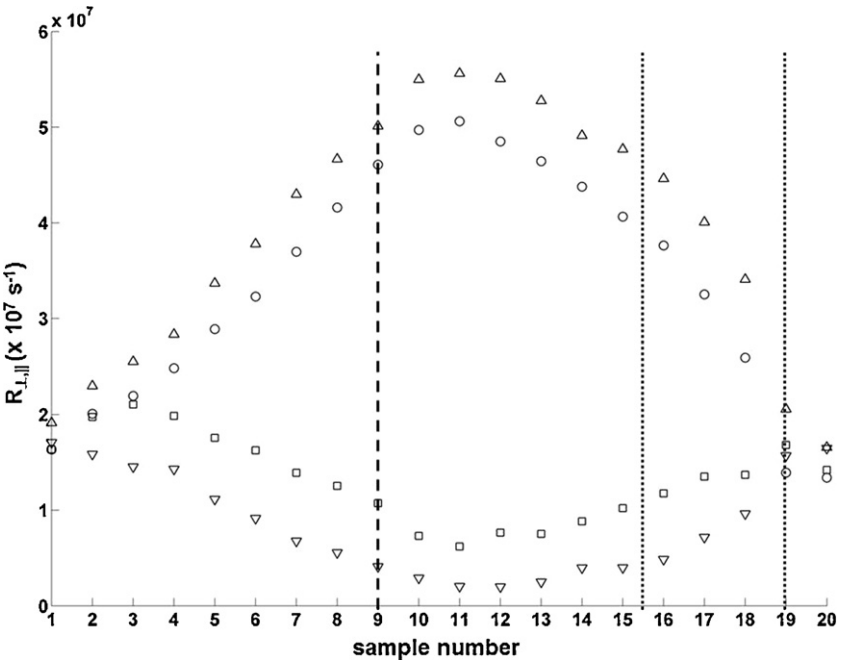

Fig. 4. The $R_\perp$ and $R_{||}$ parameter profiles for 5PC and 7PC. $R_\perp$ 5PC (circles), $R_{||}$ 5PC (squares), $R_\perp$ 7PC (up triangle), and $R_{||}$ 7PC (down triangle). The dashed line is the location of the critical point and the dotted lines are the locations of the invariant points of the three-phase region.

and overall motions (Lou et al., 2001). Needless to say, the fitting and interpretation thus depends, at least to some extent, on the nature of the model used. It is encouraging that in this work and that of Livshits et al. (2004) on a different lipid system, both show that $R_{||}/R_\perp$ decreases as one goes up the acyl chain.

3.1.1.3. Ordering tensor profiles. The S_0 profiles for all chain-labeled spin-labels are plotted in Fig. 5. Although we encountered only positive S_0, as noted above, S_2 was either positive or negative, which may reflect a preference for the molecular X_R and Y_R axes relative to the local bilayer normal, but X-band ESR spectroscopy on MOMD samples is too ambiguous for a meaningful determination. As was shown previously in a multi-frequency ESR study (Lou et al., 2001), MOMD at X-band incorporates the composite (i.e. fast and slow) motions of the acyl chains which limits the interpretation of S_2. (However, S_2 was utilized in a previous study (Chiang et al., 2004) in an attempt to estimate S_{xx} and S_{yy} from an X-band MOMD analysis, but with in conclusive results, as noted by the authors.) A substantial S_2 would either imply biaxial alignment (Lou et al., 2001) or tilting of the acyl chain (Chiang et al., 2004), but according to experiments at higher frequencies and better modeling of the motions (Lou et al., 2001), the ordering indicated by S_2 from X-band alone was unjustified. Therefore, we will not consider the S_2 results in our physical interpretation of phase dynamics and ordering, but the data is provided in Supplementary Material along with the transformation to the Cartesian representations of the order parameters.

For both the L_o and L_d phase, S_0 generally decreased with carbon position along the acyl chain. The S_0 profiles with carbon position of the L_o phase with the highest cholesterol concentration (composition 1, mole fraction cholesterol ~45%) and the L_d phase with the lowest cholesterol concentration (composition 12, mole fraction cholesterol ~5%) are plotted in Fig. 6. The trend of the order parameter decreasing with carbon position has frequently been observed before by ESR (Swamy et al., 2006; Mainali et al., 2011a,b,c; Hubbell and McConnell, 1971) and ^{2}H NMR (Lafleur et al., 1990; Bartels et al., 2008; Clarke et al., 2009). Both ESR and NMR reveal that the L_o phase has larger order parameters along the entire acyl chain than the L_d phase; however, the shape of the profiles given by the two methods is different. The profile from NMR generally has a small change in order for the top half of the chain (called the "plateau" region to about carbon 10) and a large but monotonic convex drop in order towards the end of the chain for the bottom half of the acyl chain; the shape exists for sphingomyelin, saturated and monounsaturated glycerophospholipids, and their mixtures with cholesterol. However, the profile from ESR is more linear for these lipid systems, close to what we observe. The differences observed in ordering by ESR vs. NMR are usually attributable to the shorter time-scale of ESR, so slower motions which provide additional averaging in NMR do not in ESR.

Interestingly, contrary to the general trend, S_0 was higher for 12PC than for 10PC within the L_o phase, but they converged in approaching the critical point, and they had approximately the same value near the critical point, whereas S_0 was lower for 12PC than for 10PC within the L_d phase as is typically seen (Fig. 5). This result in the L_o phase shows up as a "dip" in the order parameter profile versus carbon position at position 10 (Fig. 6), and the decrease in order within the L_d phase around position 10 and 12 shows up as a concave "bulge" (Fig. 6). A dip in order was also seen in ^{2}H NMR order parameters for DOPC, DOPC/Chol mixtures, and a diunsaturated glycerophospholipid with the cis double bonds on a single acyl chain (Warschawski and Devaux, 2005; Baenziger et al., 1991); these differences in the NMR order parameter profiles with carbon position emphasize the importance of which acyl chain (i.e. sn-1 or sn-2, unsaturated or saturated) is deuterated. This difference in the order parameter between 10PC and 12PC seems to be the result of the cis double bond of DOPC between carbon 9 and 10 and its interaction with the methyl groups at the end of the β-face of the sterol ring of cholesterol and it alkyl chain, which extends approximately between carbon 10 and 12 of the acyl chains. The cis double bond, being rigid and bent, and the protruding methyl groups could open up localized free volume in the L_o phase, whereas, within the L_d phase, the perturbation would be more diffuse. Furthermore, S_0 for 14SPM was higher than for 16PC within the L_o phase, but these order parameters were the same within the L_d phase. The difference between 14SPM and 16PC

Author's personal copy

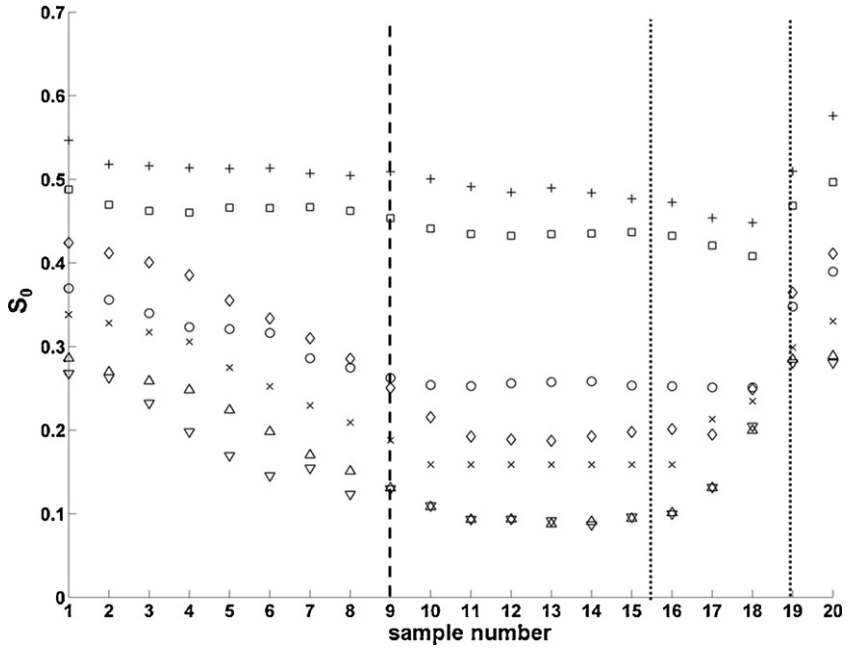

Fig. 5. The S_0 parameter profiles for the chain-labeled phospholipids. 5PC (plus sign), 7PC (squares), 10PC (circles), 12PC (diamonds), 14PC (crosses), 14SPM (up triangles), and 16PC (down triangles). The dashed line is the location of the critical point and the dotted lines are the locations of the invariant points of the three-phase region.

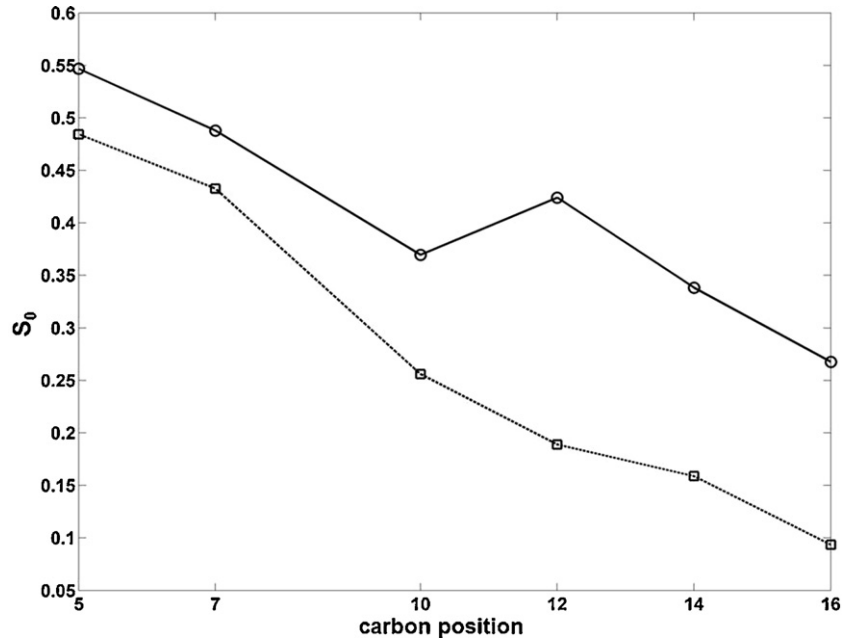

Fig. 6. The S_0 parameter versus carbon position of the nitroxide. The plot contains composition 1, a L_o phase with mole fraction cholesterol ~45% (circles, solid line), and composition 12, a L_d phase with mole fraction cholesterol ~5% (squares, dashed line).

within the L_o phase presumably reflects the stronger interaction of cholesterol with sphingomyelin than glycerophospholipids.

The S_0 parameter profiles (Fig. 5) show differences between the L_o and L_d phases with changes in composition. For most of the L_o phase (compositions 2–9), S_0 of 5PC and 7PC decrease slightly with decreasing cholesterol, but are higher and vary sharply for the L_o phases with high concentrations of SPM and cholesterol (compositions 19-1). However, also within the L_o phase, the bottom half of the acyl chains (i.e. 10PC-16PC) decrease approximately linearly and significantly with decreasing cholesterol, and increase the same way with increasing cholesterol (but 14SPM and 16PC remain constant for the L_o phase with high concentrations of SPM and cholesterol, compositions 19-1). For the L_d phase (compositions 10–15) S_0 of all carbon positions remained approximately constant, nearly independent of composition.

3.1.1.4. Summary: Emerging model. The dynamic and order parameters of the chain-labeled spin-labels taken together yield an intriguing picture of the L_o and L_d phases. For the acyl chain within both the L_o and L_d phases, the off axial rotation (i.e. $R_\perp$) and alignment with the bilayer normal (i.e. S_0) decrease with carbon position from top to bottom. For the L_d phase, the alignment decreases greatly with carbon position but does not vary much with composition. The rotation also does not change much (less than an order

Author's personal copy

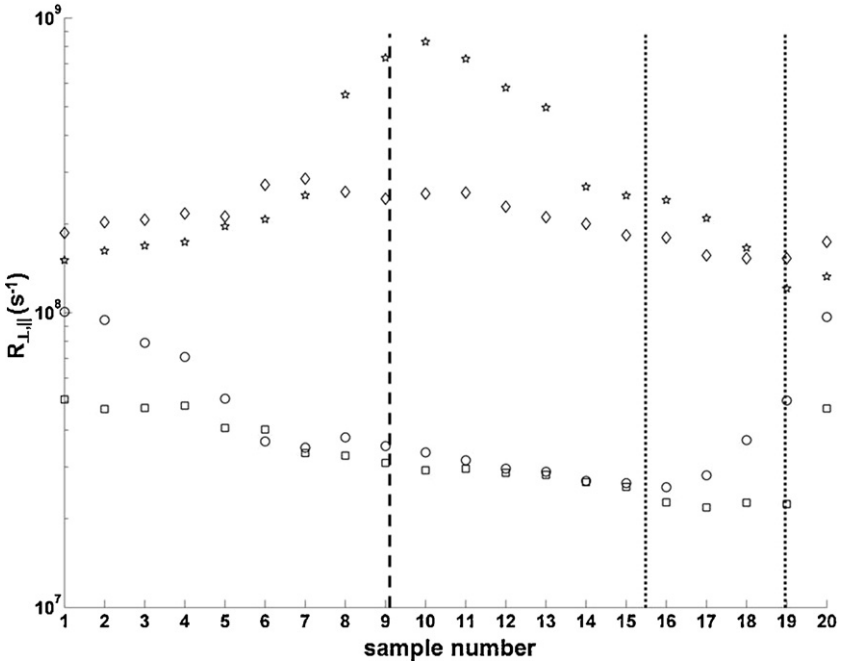

Fig. 7. The $R_\perp$ and $R_{||}$ parameter (log-scale) profiles for the headgroup-labeled phospholipids, DPPTC and SPMHEAD. $R_\perp$ DPPTC (circles), $R_{||}$ DPPTC (diamonds), $R_\perp$ SPMHEAD (squares), and $R_{||}$ SPMHEAD (stars). The dashed line is the location of the critical point and the dotted lines are the locations of the invariant points of the three-phase region.

of magnitude) but does vary with cholesterol. For the L_o phase, the structures between the top and bottom halves of the acyl chains are different. The off-axial rotation for the top half decreases greatly with increasing cholesterol; however, the rotation for the bottom half either does not change much or increases (especially at the ends) with increasing cholesterol. In addition, the top half of the acyl chain is highly aligned along the bilayer normal and changes little with cholesterol concentration; however, for the bottom half, the alignment with the bilayer normal increases with increasing cholesterol. Therefore, within the L_o phase, cholesterol straightens the top half of the acyl chains and decreases off-axial rotation because the ring system induces a greater tendency for trans bonds; concurrently, cholesterol generally increases the motion of the bottom half of the acyl chains because its branched alkyl chain allows free volume for gauche bonds. This rigidifying effect for the top half of the acyl chains and the fluidizing effect for the bottom half caused by cholesterol has previously been observed by ESR in comparing pure DMPC in the L_d phase and 1/1 DMPC/cholesterol mixture in the L_o phase (Mainali et al., 2011a,b).

3.1.2. The headgroup-labeled spin-labels

The two headgroup-labeled spin-labels used in this work were DPPTC, a glycerophospholipid, and SPMHEAD, a sphingomyelin. Although they are very similar within the hydrocarbon region (i.e. equal chain lengths), the interfacial and headgroup regions are completely different (Fig. 1). DPPTC has a large choline headgroup and SPMHEAD has a small nitroxide moiety as the headgroup. The $R_\perp$ and $R_{||}$ profiles of both spin-labels are plotted in Fig. 7. For all compositions and for both spin-labels $R_{||}$ was greater than $R_\perp$. The $R_\perp$ profiles of both spin-labels have no discernible dependence on composition, but are higher in L_o phases (compositions 1–9) than L_d phases (compositions 9–15). Interestingly, the $R_\perp$ of DPPTC is significantly larger than for SPMHEAD with the L_o phase of high cholesterol concentration (compositions 1–4, 20, mole fraction cholesterol >∼40%). Unlike the $R_\perp$profiles, the $R_{||}$ profiles of both spin-labels are roughly dependent on the phospholipid concentration by increasing with increasing/decreasing DOPC/SPM (compositions 1–10, 19–20) and decreasing with increasing/decreasing SPM/DOPC (compositions 10–15). Since the interface of DOPC has weak intermolecular interactions because of a lack of hydrogen-bonding, an increase in its concentration, along with a decrease in SPM and cholesterol, allows more free volume for the headgroup to rotate. However, the interface of SPM has strong intermolecular interactions with each other and DOPC because of extensive hydrogen-bonding capability; therefore, an increase in its concentration, along with an increase in cholesterol and decrease in DOPC, allows less free volume for the headgroup to rotate. Given the greater change in $R_{||}$ these effects seem more pronounced for SPMHEAD than DPPTC. Therefore, within the L_o phase the headgroup has more free volume to move along the bilayer surface than within the L_d phase, as predicted by the umbrella model (Huang et al., 1999).

The S_0 parameter profiles of DPPTC and SPMHEAD are plotted in Fig. 8. Because of the cyclical permutation of the magnetic frame, $X_m \,||\, Z_R$, S_0 specifies the alignment of the magnetic x-axis of the nitroxide with the bilayer normal. For nearly all compositions S_0 of SPMHEAD is ≥ DPPTC; this reflects the fact that the nitroxide moiety of SPMHEAD is attached directly to the phosphate, which is probably more restrictive in range of motion for sphingomyelins than glycerophospholipids because of hydrogen-bonding. S_0 of SPMHEAD is larger for the L_o phase than the L_d phase most likely because alignment with the bilayer normal is the more efficient packing for a small headgroup that cannot shield cholesterol from water. However, S_0 of DPPTC for the L_o phase is smaller than for the L_d phase of high cholesterol concentration (compositions 1–4, 19–20), implying a greater range of motion away from the bilayer normal and towards the bilayer surface in the L_o phase. For a few compositions within the L_o phase (compositions 5–9), S_0 was larger than in the L_d phase. This local maximum in S_0 of DPPTC coincides with a local maximum in S_0 of CSL (see below), and, in fact, trend similarly in the L_o phase, suggesting a relationship between the ordering of the choline headgroup and cholesterol. The order parameter profile for SPMHEAD shows no discernible trend with cholesterol concentration; however, for most of the L_o phase (compositions 19-7), S_0

Author's personal copy

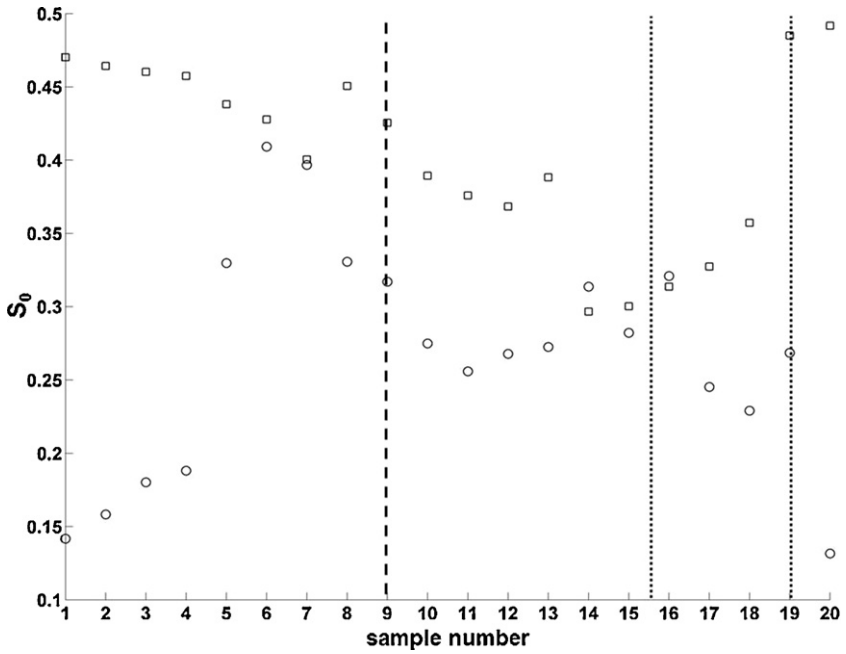

Fig. 8. The S_0 parameter profiles for DPPTC (circles) and SPMHEAD (squares). The dashed line is the location of the critical point and the dotted lines are the locations of the invariant points of the three-phase region.

of DPPTC decreases with increasing cholesterol (compositions 19-1) and increases with decreasing cholesterol (compositions 1–7). Also, generally within the L_d phase, S_0 of DPPTC decreases with decreasing cholesterol (compositions 9–11) and increases with increasing cholesterol (compositions 11–15). Headgroup size of SPM and glycerophospholipidsis important in its interactions with cholesterol and are integral to the umbrella model (Terova et al., 2005; Bjorkbom et al., 2010). In agreement, we observed that the ordering of a small headgroup (SPMHEAD) does not depend on cholesterol concentration but a large headgroup (DPPTC) does. Also, we observed that the choline headgroup (DPPTC) in the L_o phase has both a greater magnitude and range of motion along the bilayer surface (i.e. away from the bilayer normal) than in the L_d phase presumably to shield cholesterol from water; an observation predicted by the umbrella model.

3.1.3. CSL

The nitroxide labeled cholestane spin-label (CSL) is a cholesterol analogue and is used to study the dynamics and ordering of cholesterol. The $R_\perp$ and $R_{||}$ profiles of CSL are plotted in Fig. 9. For all compositions $R_{||}$ was at least an order of magnitude greater than $R_\perp$, but the difference between the parameters was greater for the L_o phase (compositions 1–9, 19–20) than the L_d phase (compositions 9–15). $R_{||}$ is only a little larger in the L_d phase than in the L_o phase. Within the L_o phase, $R_{||}$ increases with decreasing/increasing SPM/DOPC where it reaches a local maximum at sample 10, which has the highest DOPC and lowest SPM concentration; afterwards, within the L_d phase, $R_{||}$ dips with decreasing cholesterol to around composition 12, then increases approaching the three-phase region with increasing cholesterol. Within the L_o phase, $R_\perp$ increases by almost an order of magnitude with decreasing/increasing SPM/DOPC approaching the critical point and exhibits a discontinuity near the critical point (between compositions 8 and 9). Within the L_d phase $R_\perp$ is constant with decreasing cholesterol, exhibits a discontinuity between compositions 12 and 13, and then decreases with increasing cholesterol. Moreover, CSL dynamics correlates with the SPM concentration within the L_o phase, which is consistent with the preferential interaction between cholesterol and sphingomyelin (Halling et al., 2008).

The S_0 order parameter profile of CSL is plotted in Fig. 10. Because of the cyclical permutation of the magnetic frame, Y_m || Z_R, S_0 specifies the alignment of the axis perpendicular to the magnetic x-axis and z-axis of the nitroxide with the bilayer normal. For most of the L_o phase S_0 increases with decreasing SPM concentration (compositions 19-7), but after composition 7 (mole fraction cholesterol ~33%) S_0 decreases towards the critical point. Within the L_d phase S_0 decreases slightly with decreasing cholesterol (compositions 9–12), but S_0 decreases sharply with increasing cholesterol (compositions 12–15). In mixtures of DMPC/cholesterol, POPC/cholesterol, DMPC/POPC/cholesterol, and DLPC/DPPC/cholesterol the S_0 order parameter increased with increasing cholesterol in going from the L_d phase to the L_o phase but reached a plateau around mole fraction cholesterol ~33% (Chiang et al., 2004; Shin and Freed, 1989), which is similar to our observation (compositions 12-7). As with its dynamics, CSL ordering is dependent on the SPM concentration within the L_o phase. Moreover, the most significant observation is that S_0 changes with SPM concentration in the L_o phase and cholesterol concentration in the L_d phase. In addition, CSL is more disordered in a L_o phase containing a high concentration of SPM and cholesterol than in a L_d phase containing low concentrations. Interestingly, the transformation of S_0 and S_2 of CSL into the Cartesian representation of the order parameters (see Supplementary Material) shows a large negative S_{zz} (i.e. alignment of Z_m with the bilayer normal) within the L_o phase, which suggests a strong tilt towards the hydrophobic interior of the bilayer or a “cutting” motion about the axis perpendicular to the steroid ring (Barnes and Freed, 1998). A local biaxial alignment was observed for CSL in DMPC/DMPS mixtures analyzed with multi-frequency ESR spectroscopy and explained by void formation from inefficient packing of the PS headgroups (Barnes and Freed, 1998).A similar reorientation of CSL may be occurring in the L_o phase of our system because of void formation from both headgroup expansion and acyl chain condensation, although as we have remarked, there are considerable uncertainties into our determination of S_2.

Author's personal copy

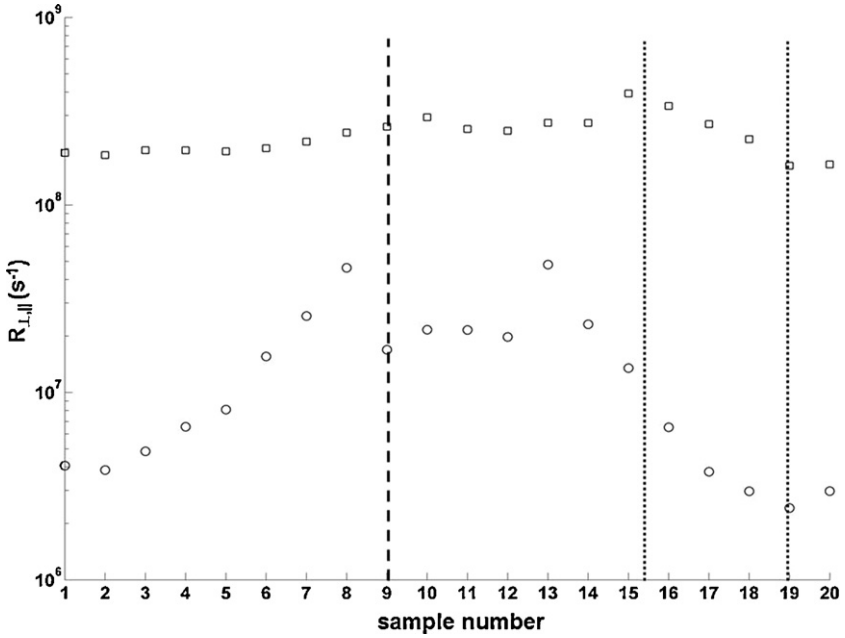

Fig. 9. The $R_\perp$ (circles) and $R_\parallel$ (squares) parameter (log-scale) profiles for CSL. The dashed line is the location of the critical point and the dotted lines are the locations of the invariant points of the three-phase region.

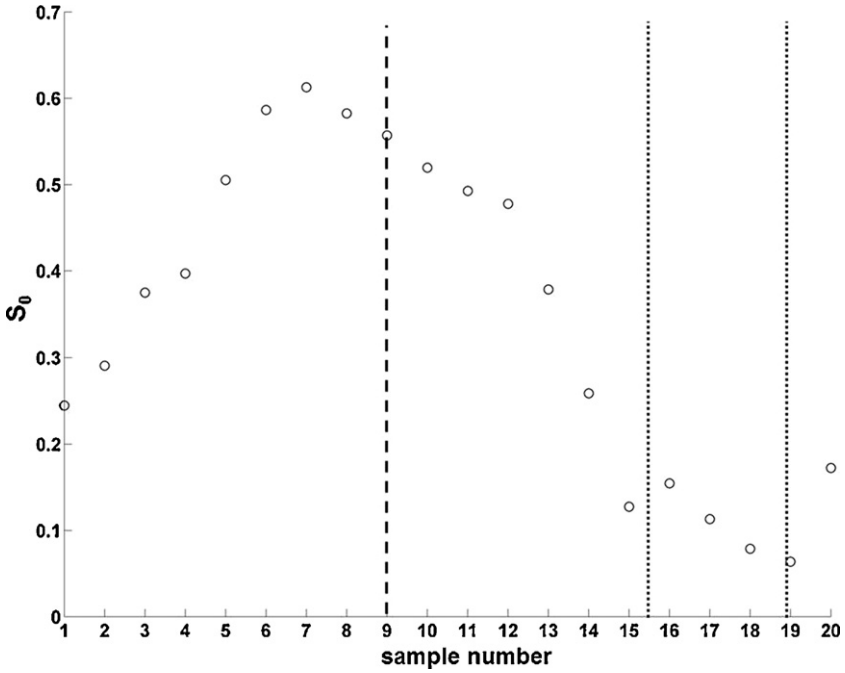

Fig. 10. The S_0 parameter profile for CSL. The dashed line is the location of the critical point and the dotted lines are the locations of the invariant points of the three-phase region.

3.2. Coexistence of L_o and L_d phases

The key advantage of choosing the SPM/DOPC/Chol lipid system to study the structure of the L_o and L_d phases is the knowledge of both the phase boundaries and the tie-line field (Fig. 2). Given that the two-domain model has been used for the structure of biomembranes, the tie-line field enables us to compare the structure of coexisting L_o and L_d phases. Within the gel phase of sphingomyelin and glycerophospholipids, the lipids are efficiently packed with the acyl chains existing primarily in the all trans configuration and the headgroups occupying a minimum volume. The transition from the gel phase to the L_d phase mainly occurs within the hydrocarbon region. Gauche isomers distribute along the entire acyl chain, but more frequently towards the ends, and increase their cross-sectional area, while the volume of the headgroup increases slightly (Nagle and Tristram-Nagle, 2000; Marsh, 2010). The acyl chains have a very high degree of dynamics, as evidenced by ESR studies with chain-labeled spin-labels, showing a positional distribution of the nitroxide centered around its carbon position but extending a significant distance away (Vogel et al., 2003), even suggesting a small but finite probability that the nitroxide of 16PC can reach the interface.

Author's personal copy

In this regard, we visualize the acyl chains within the hydrocarbon region of the L_d phase as an "entanglement of snakes", which is similar to the bulk phase of linear hydrocarbons, but with a lateral pressure profile decreasing along the chains from the interface that aligns them, on average, with the bilayer normal. On the other hand, the L_o phase, which has only been observed in mixtures with cholesterol, has significant structural differences from the L_d phase. First, the headgroup occupies more volume, aligning more towards the bilayer surface and with a greater rotation. Second, the steroid ring system of cholesterol condenses the top half of the acyl chains into an all trans configuration and decreases its rotation within the bilayer plane; however, the alkyl chain of cholesterol disorders the bottom half of the chains and increases its rotation (Mainali et al., 2011a,b). The combination of the expansion of the headgroup and condensation of the top half of the acyl chains could possibly form a pocket of free volume or void space, allowing the long molecular axis of cholesterol a considerable amount of reorientation (Barnes and Freed, 1998).

With this structural picture in mind, an analysis of the coexisting L_o and L_d phases revealed by the tie-line field of the SPM/DOPC/cholesterol lipid system can be made. A central tie-line of the field connects a L_o phase with a high concentration of cholesterol (near composition 1) and a L_d phase with a low concentration of cholesterol (near composition 12). The acyl chain structure for this L_o phase has the top half condensed in the all trans configuration due to low free volume and slow motion, and the bottom half is expanded due to its higher free volume and fast motion. This is in agreement with a very recent MD study (Plesnar et al., 2012). The entire acyl chain is predominantly ordered along the bilayer normal. In addition, the headgroup structure of this L_o phase is expanded with high off axial rotation and a large range of motion towards the bilayer surface. On the contrary, the acyl chain structure of the L_d phase of this central tie-line is disordered, except for the very top which is ordered along the bilayer normal, with fast dynamics along the entire chain. Also, the headgroup structure of this L_d phase has a predominant alignment with and motion around the bilayer normal. Furthermore, the difference in thickness between these L_o and L_d phases is probably high.

As we move toward the critical point from this central tie-line, the acyl chain dynamics of the L_o phase changes with composition so that the top expands and the bottom condenses. The alignment of the entire acyl chain with the bilayer normal decreases, but the disordering is greater for the bottom half than for the top half. With this change in composition in the L_o phase, dynamics and ordering trend oppositely for the top of the acyl chain (i.e. high ordering, low dynamics), but they trend together for the bottom (i.e. low ordering, low dynamics). Also, as the L_o phase approaches the critical point, the headgroup condenses with increasing rotation around the bilayer normal and decreasing rotation along the bilayer surface, while the alignment along the bilayer normal generally increases. This structure of the L_o phase is consistent with approaching the structure of the L_d phase.

As the composition of the L_d phase approaches the critical point, off-axial rotation decreases along the entire chain, but the dominant alignment along the bilayer normal does not change or slightly increases. Also, for the headgroup of the L_d phase, the rotation along the bilayer surface increases, while the alignment with the bilayer normal increases slightly. The structure of the L_d phase is generally consistent with approaching the structure of the L_o phase, but does not yet show the bifurcation of the acyl chain structure characteristic of the L_o phase. Moreover, the combined effect when approaching the critical point is that the thickness of the L_o phase likely decreases and the thickness of the L_d phase likely increases until at the critical point the two phases have the same thickness.

As we move toward the three-phase region from this central tie-line, the change in the structure of the L_o and L_d phases show characteristics of the L_d or L_o phase and the gel phase appearing. The acyl chain dynamics of the L_o phase changes with composition so that the top expands and the bottom condenses; the alignment with the bilayer normal for most of the acyl chain, while still high, decreases rapidly, except for the end which remains constant. Also, the headgroup of the L_o phase condenses with slightly decreasing rotation around the bilayer normal and rapidly decreasing rotation along the bilayer surface, while the alignment with the bilayer normal greatly increases. The structure of the L_o phase is consistent with approaching both the L_d and gel phases because of the headgroup condensation and the loss of bifurcation of the acyl chain structure. As the composition of the L_d phase approaches the three-phase region, off-axial rotation decreases along the entire chain, but the dominant alignment with the bilayer normal does not change. For the headgroup of the L_d phase, both rotation around the bilayer normal and along the bilayer surface decrease, while alignment with the bilayer normal increases slightly. The structure of the L_d phase is consistent with approaching both the L_o and gel phases because of both acyl chain and headgroup condensation with dominant headgroup alignment along the bilayer normal.

The phase diagrams of the DPPC/DOPC/cholesterol (Veatch et al., 2004), palmitoyl-SPM/POPC/cholesterol (Livshits et al., 2010), and DSPC/DOPC/cholesterol (Zhao et al., 2007; Heberle et al., 2010) lipid systems are comparable to the phase diagram of our system, because of the lipid similarities and the existence of phase boundaries and tie-lines for the $L_o + L_d$ coexistence region. The closed coexistence regions (i.e. not intersecting a binary system) for all these ternary systems contain a critical point and a bordering three-phase region; however, the location of the critical point and the slope of the tie-lines are different. For the SPM containing systems (palmitoyl-SPM and ours), the mole fraction of cholesterol at the critical point is ~20% and the tie-line slopes are ~60°, and for the DPPC and DSPC systems the mole fraction of cholesterol is ~40% and the slopes are ~30°. However, for the DSPC system S_0 parameters of 16PC for two L_o and L_d phases were qualitatively the same as our observations (Heberle et al., 2010). The difference between the tie-line slopes and location of the critical point, which are related, between the sphingomyelin and glycerophospholipid systems most likely has to do with the stronger interaction of cholesterol for sphingomyelin than glycerophospholipids. Because of this preferred interaction it takes less sphingomyelin and more glycerophospholipids per mole of cholesterol to form the L_o phase; therefore, the tie-lines for the sphingomyelin systems are ~60° (i.e. mole fraction sphingomyelin ~ the same between L_o and L_d phases) and the tie-lines for the glycerophospholipids are ~ 30° (i.e. mole fraction glycerophospholipid $L_o > L_d$).

4. Conclusions

The main objective of this work was to elucidate the dynamic molecular structure of the coexisting L_o and L_d phases within the SPM/DOPC/Chol model lipid system. The use of 10 different spin-labels labeled along the acyl chain and within the headgroup of phospholipids, as well as a labeled cholesterol analogue, allowed both the hydrophobic and hydrophilic sections of the bilayer of this model system to be analyzed. ESR spectra were obtained at 20 compositions along the $L_o + L_d$ coexistence curve and fit to extract the dynamic molecular parameters. The analysis was complemented with the known locations of the critical point and invariant points of the neighboring three-phase region, which divide the coexistence curve into the L_o and L_d phase boundaries. This set of data allowed us to draw three basic conclusions: (1) the condensing effect of cholesterol was indirectly observed, (2) substantial support for the umbrella model was provided, and (3) a continuous transition in both dynamics and ordering occurs in the acyl chains of

Author's personal copy

phospholipids within L_o and L_d phases approaching and traversing through the critical point.

The condensing effect of cholesterol can be seen in the results for the chain-labeled spin-labels. Essentially, our model for the condensing effect is that the rigid sterol ring of cholesterol (extending approximately from carbon 1–10) entropically forces the top half of the acyl chains to adopt more trans bonds as the concentration of cholesterol increases, and the increase in trans bonds causes condensation, while concurrently the bottom half adopts more gauche bonds. The reason against the ethalpic formation of a saturated lipid/cholesterol compound is that if this occurred there would not be a bifurcation of the acyl chain in dynamics and ordering between the top and bottom. Also, there would be similar trends in dynamics and ordering between the chain-labeled spin-labels and CSL, which we do not observe.

The experimental support for the umbrella model can be seen in the results for the headgroup-labeled spin-label DPPTC. We observed the headgroup of DPPTC, similar to phosphatidylcholines, within the L_o phase occupy a greater volume along the bilayer surface than in the L_d phase to shield cholesterol from water, as predicted by the umbrella model. In addition, we observed that the much smaller headgroup of SMHEAD exhibits both slower dynamics and reduced ordering within the L_o phase than DPPTC. Therefore, in agreement with the model, a larger headgroup size of the phospholipid makes a better umbrella.

In approaching and traversing through the critical point, we observe a continuous transition in dynamics and ordering of the phospholipid acyl chains. When starting from the coexisting L_o phase of maximal cholesterol concentration, the difference between the top and bottom halves of the acyl chains decreases in off axial dynamics (i.e. top increases, bottom decreases) and increases in axial ordering (i.e. top constant, bottom decreases) approaching the critical point. When starting from the coexisting L_d phase of minimal cholesterol concentration, the off axial dynamics of the entire acyl chain decreases, while the axial ordering of the entire acyl chain is constant or increases slightly approaching the critical point. These two phase structures smoothly and continuously change into one another when traversing through the critical point. Moreover, presumably at the critical point, long-range fluctuations between the bifurcated acyl chain structure of the L_o phase and the undivided and cooperative acyl chain structure of the L_d phase exist, but we did not attempt to study this.

Acknowledgments

We thank Dr. Boris Dzikovski for a critical reading of this manuscript and for helpful advice. This work was supported by grants from the National Institute of Health/National Institute of Biomedical Imaging and Bioengineering R01EB003150 and National Center for Research Resources P41RR016292, as well as the National Institute of General Medical Sciences, P41GM103521.

Appendix A. Supplementary data

Supplementary data associated with this article can be found, in the online version, at doi:10.1016/j.chemphyslip.2012.02.009.

References

Ayuyan, A.G., Cohen, F.S., 2008. Raft composition at physiological temperature and pH in the absence of detergents. Biophys. J. 94, 2654–2666.

Baenziger, J.E., Jarrell, H.C., Hill, R.J., Smith, I.C.P., 1991. Average structural and motional properties of a diunsaturated acyl chain in a lipid bilayer: effects of two cis-unsaturated double bonds. Biochemistry 1991 (30), 894–903.

Barnes, J.P., Freed, J.H., 1998. Dynamics and ordering in mixed model membranes of dimyristoylphophatidylcholine and dimyristoylphosphatidylserine: a 250-GHz electron spin resonance study using cholestane. Biophys. J. 75, 2532–2546.

Bartels, T., Lankalapalli, R.S., Bittman, R., Beyer, K., Brown, M.F., 2008. Raftlike mixtures of sphingomyelin and cholesterol investigated by solid-state ^{2}H NMR spectroscopy. J. Am. Chem. Soc. 130, 14521–14532.

Baumgart, T., Hammond, A.T., Sengupta, P., Hess, S.T., Holowka, D.A., Baird, B.A., Webb, W.W., 2007. Large-scale fluid/fluid phase separation of proteins and lipids in giant plasma membrane vesicles. Proc. Natl. Acad. Sci. U.S.A. 104, 3165–3170.

Bjorkbom, A., Rog, T., Kaszuba, K., Kurita, M., Yamaguchi, S., Lonnfors, M., Nyholm, T.K.M., Vattulainen, I., Katsumura, S., Slotte, J.P., 2010. Effect of sphingomyelin-headgroupsize on molecular properties and interactions with cholesterol. Biophys. J. 99, 3300–3308.

Buboltz, J.T., Feigenson, G.W., 1999. A novel strategy for the preparation of liposomes: rapid solvent exchange. Biochim. Biophys. Acta 1417, 232–245.

Budil, D.E., Lee, S., Saxena, S., Freed, J.H., 1996. Nonlinear-least-squares analysis of slow-motion EPR spectra in one and two dimensions using a modified Levenberg-Marquardt algorithm. J. Magn. Reson. A 120, 155–189.

Chiang, Y.W., Shimoyama, Y., Feigenson, G.W., Freed, J.H., 2004. Dynamic molecular structure of DPPC-DLPC-Cholesterol Ternary Lipid System by Spin-Label Electron Spin Resonance. Biophys. J. 87, 2483–2496.

Clarke, J.A., Seddon, J.M., Law, R.V., 2009. Cholesterol containing model membranes studied by multinuclear sold state NMR spectroscopy. Soft Matter 5, 369–378.

Collado, M.I., Goni, F.M., Alonso, A., Marsh, D., 2005. Domain formation in sphingomyelin/cholesterol mixed membranes studied by spin-label electron spin resonance spectroscopy. Biochemistry 44, 4911–4918.

Daly, T.A., Wang, M., Regen, S.L., 2011. The origin of cholesterol's condensing effect. Langmuir 27, 2159–2161.

Earle, K.A., Moscicki, J.K., Ge, M., Budil, D.E., Freed, J.H., 1994. 250-GHz Electron spin resonance studies of polarity gradients along the aliphatic chains in phospholipid membranes. Biophys. J. 66, 1213–1221.

Edholm, O., Nagle, J.F., 2005. Areas of molecules in membranes consisting of mixtures. Biophys. J. 89, 1827–1832.

Feigenson, G.W., 2009. Phase diagrams and lipid domains in multicomponent lipid bilayer mixtures. Biochim. Biophys. Acta 1788, 47–52.

Ge, M., Field, K.A., Aneja, R., Holowka, D., Baird, B., Freed, J.H., 1999. Electron spin resonance characterization of liquid ordered phase of detergent-resistant membranes from RBL-2H3 cells. Biophys. J. 77, 925–933.

Ge, M., Freed, J.H., 1998. Polarity profiles in oriented and dispersed phosphatidylcholine bilayers are different: an electron spin resonance study. Biophys. J. 74, 910–917.

Ge, M., Freed, J.H., 2003. Hydration, structure, and molecular interactions in the headgroup region of dioleoylphosphatidylcholine bilayers: an electron spin resonance study. Biophys. J. 85, 4023–4040.

Ge, M., Freed, J.H., 2009. Fusion peptide from influenza hemmagglutinin increases membrane surface order: an electron-spin resonance study. Biophys. J. 96, 4925–4934.

Ge, M., Freed, J.H., 2011. Two conserved residues are important for inducing highly ordered membrane domains by the transmembrane domain of influenza hemagglutinin. Biophys. J. 100, 90–97.

Ge, M., Gidwani, A., Brown, H.A., Holowka, D., Baird, B., Freed, J.H., 2003. Ordered and disordered phases coexist in plasma membrane vesicles of RBL-2H3 mast cells. An ESR study. Biophys. J. 85, 1278–1288.

Goni, F.M., Alonso, A., Bagatolli, L.A., Brown, R.E., Marsh, D., Prieto, M., Thewalt, J.L., 2008. Phase diagrams of lipid mixtures relevant to the study of membrane rafts. Biochim. Biophys. Acta 1781, 665–684.

Halling, K.K., Ramstedt, B., Nystrom, J.H., Slotte, J.P., Nyholm, T.K.M., 2008. Cholesterol interactions with fluid-phase phospholipids: effect on the lateral organization of the bilayer. Biophys. J. 95, 3861–3871.

Heberle, F.A., Wu, J., Goh, S.L., Petruzielo, R.S., Feigenson, G.W., 2010. Comparison of three ternary lipid bilayer mixtures: FRET and ESR reveal nanodomains. Biophys. J. 99, 3309–3318.

Huang, J., Buboltz, J.T., Feigenson, G.W., 1999. Maximum solubility of cholesterol in phosphatidylcholine and phosphatidylethanolamine bilayers. Biochim. Biophys. Acta 1417, 89–100.

Hubbell, W.L., McConnell, H.M., 1971. Molecular motion in spin-labeled phospholipids and membranes. J. Am. Chem. Soc. 93, 314–326.

Hung, W.C., Lee, M.T., Chen, F.Y., Huang, H.W., 2007. The condensing effect of cholesterol in lipid bilayers. Biophys. J. 92, 3960–3967.

Kaiser, H., Lingwood, D., Levental, I., Sampaio, J.L., Kalvodova, L., Rajendran, L., Simons, K., 2009. Order of lipid phases in model and plasma membranes. Proc. Natl. Acad. Sci. U.S.A. 106, 16645–16650.

Klauda, J.B., Roberts, M.F., Redfield, A.G., Brooks, B.R., Pastor, R.W., 2008. Rotation of lipids in membranes: molecular dynamics simulation, 31P spin-lattice relaxation, and rigid-body dynamics. Biophys. J. 94, 3074–3083.

Korstanje, L.J., Van Faassen, E.E., Levine, Y.K., 1989. Slow-motion ESR study of order and dynamics in oriented lipid multibilayers: effects of unsaturation and hydration. Biochim. Biophys. Acta 980, 225–233.

Kurad, D., Jeschke, G., Marsh, D., 2003. Lipid membrane polarity profiles by high-field EPR. Biophys. J. 85, 1025–1033.

Lafleur, M., Cullis, P.R., Bloom, M., 1990. Modulation of the orientation order profile of the lipid acyl chain in the Lα phase. Eur. Biophys. J. 19, 55–62.

Levental, I., Grzybek, M., Simons, K., 2011. Raft domains of variable properties and compositions in plasma membrane vesicles. Proc. Natl. Acad. Sci. U.S.A. 108, 11411.

Lingwood, D., Simons, K., 2010. Lipid rafts as a membrane-organizing principle. Science 327, 46–50.

Author's personal copy

Livshits, V.A., Demisheva, I.V., Marsh, D., 2010. Self-organization and phase structure of ternary lipid membranes: a spin label ESR study. Nanotechnol. Russia 5, 601–610.
Livshits, V.A., Kurad, D., Marsh, D., 2004. Simulation studies on high-field EPR spectra of lipid spin labels in cholesterol-containing membranes. J. Phys. Chem. B 108, 9403–9411.
Lou, Y., Ge, M., Freed, J.H., 2001. A multifrequency ESR study of the complex dynamics of membranes. J. Phys. Chem. B 105, 11053–11056.
Montes, L., Alonso, A., Goni, F.M., Bagatolli, L.A., 2007. Giant unilamellar vesicles electroformed from native membranes and organic lipid mixtures under physiological conditions. Biophys. J. 93, 3548–3554.
Mainali, L., Felix, J.B., Hyde, J.S., Subczynski, W.K., 2011a. Membrane fluidity profiles as deduced by saturation-recovery EPR measurements of spin-lattice relaxation time of spin labels. J. Magn. Reson. 212, 418–425.
Mainali, L., Raguz, M., Subczynski, W.K., 2011b. Phase-separation and domain-formation in cholesterol-sphingomyelin mixture: pulse-EPR oxygen probing. Biophys. J. 101, 837–846.
Mainali, L., Raguz, M., Subczynski, W.K., 2011. Phases and domains in sphingomyelin-cholesterol membranes: structure and properties using EPR spin-labeling methods. Eur. Biophys. J., doi:10.1007/s00249-011-0766-4, URL: www.springerlink.com/content/k429236532w034w8/.
Mannock, D.A., Lewis, R.N.A.H., McMullen, T.P.W., McElhaney, R.N., 2010. The effect of variations in phospholipid and sterol structure on the nature of lipid-sterol interactions in lipid bilayer model membranes. Chem. Phys. Lipids 163, 403–448.
Marsh, D., 2009. Cholesterol-induced fluid membrane domains: a compendium of lipid-raft ternary phase diagrams. Biochim. Biophys. Acta 1788, 2114–2123.
Marsh, D., 2010. Molecular volumes of phospholipids and glycolipids in membranes. Chem. Phys. Lipids 163, 667–677.
Nagle, J.F., Tristram-Nagle, S., 2000. Structure of lipid bilayers. Biochim. Biophys. Acta 1469, 159–195.
Plesnar, E., Subczynski, W.K., Pasenkiewicz-Gierula, M., 2012. Saturation with cholesterol increases vertical order and smoothes the surface of the phosphatidylcholine bilayer: a molecular simulation study. Biochim. Biophys. Acta 1818, 520–529.
Quinn, P.J., Wolf, C., 2009. The liquid-ordered phase in membranes. Biochim. Biophys. Acta 1788, 33–46.
Radhakrishnan, A., McConnell, H.M., 1999. Condensed complexes of cholesterol and phospholipids. Biophys. J. 77, 1507–1517.
Rog, T., Pasenkiewicz-Gierula, M., Vattulainen, I., Karttunen, M., 2009. Ordering effects of cholesterol and its analogues. Biochim. Biophys. Acta 1788, 97–121.
Shin, Y.K., Freed, J.H., 1989. Thermodynamics of phosphatidylcholine-cholesterol mixed model membranes in the liquid crystalline state studied by the orientational order parameter. Biophys. J. 56, 1093–1100.
Smith, A.K., Buboltz, J.T., Spink, C.H., Feigenson, G.W., 2003. Phase behavior of the raft mixture SPH/DOPC/cholesterol. Biophys. J. 84, 372a.
Smith, A.K., Freed, J.H., 2009. Determination of tie-line fields for coexisting lipid phases: an ESR study. J. Phys. Chem. B 113, 3957–3971.
Swamy, M.J., Ciani, L., Ge, M., Smith, A.K., Holowka, D., Baird, B., Freed, J.H., 2006. Coexisting domains in the plasma membranes of live cells characterized by spin-label ESR spectroscopy. Biophys. J. 90, 4452–4465.
Terova, B., Heczko, R., Slotte, J.P., 2005. On the importance of the phosphocholine methyl groups for sphingomyelin/cholesterol interactions in membranes: a study with ceramide phosphoethanolamine. Biophys. J. 88, 2661–2669.
Veatch, S., Keller, S., 2005. Seeing spots: complex phase behavior in simple membranes. Biochim. Biophys. Acta 1746, 172–185.
Veatch, S.L., Polozov, I.V., Gawrisch, K., Keller, S.L., 2004. Liquid domains in vesicles investigated by NMR and fluorescence microscopy. Biophys. J. 86, 2910–2922.
Veiga, M.P., Arrondo, J.L.R., Goni, F.M., Alonso, A., Marsh, D., 2001. Interaction of cholesterol with sphingomyelin in mixed membranes containing phosphatidylcholine, studied by spin-label ESR and IR spectroscopies. A possible stabilization of gel-phase sphingolipid domains by cholesterol. Biochemistry 40, 2614–2622.
Vogel, A., Scheidt, H.A., Huster, D., 2003. The distribution of lipid attached spin probes in bilayers: application to membrane protein topology. Biophys. J. 85, 1691–1701.
Warschawski, D.E., Devaux, P.F., 2005. Order parameters of unsaturated phospholipids in membranes and the effect of cholesterol: a ^{1}H–^{13}C solid-state NMR study at natural abundance. Eur. Biophys. J. 34, 987–996.
Zhang, Z., Fleissner, M.R., Tipikin, D.S., Liang, Z., Moscicki, J.K., Earle, K.A., Hubbell, W.L., Freed, J.H., 2010. Multifrequency electron spin resonance study of the dynamics of spin labeled T4 lysozyme. J. Phys. Chem. B 114, 5503–5521.
Zhao, J., Wu, J., Heberle, F.A., Mills, T.T., Klawitter, P., Huang, G., Costanza, G., Feigenson, G.W., 2007. Phase studies of model biomembranes: complex behavior of DSPC/DOPC/cholesterol. Biochim. Biophys. Acta 1768, 2764–2776.